Steel and Composite Structures, *Vol. 53, No. 3 (2024) 271-283*
https://doi.org/10.12989/scs.2024.53.3.271

Study on the technology of ribbed angle steel reinforcement for crack at rib-to-deck welds

Yuqiang Gao, Zhongqiu Fu*, Xuekun Cao and Bohai Ji

College of Civil and Transportation Engineering, Hohai University, No. 1 Xikang Road, Nanjing, China

(Received October 5, 2024, Revised October 26, 2024, Accepted October 28, 2024)

Abstract. The reinforcement technology for rib-to-deck weld cracks in orthotropic steel deck should be both efficient and lightweight, particularly for multi-crack reinforcement within a single compartment, to avoid adding excessive weight that could affect the structural stress. In this paper, a lightweight reinforcement technology using ribbed angle steel was proposed. By conducting tests and numerical simulations, the reinforcement effect of ribbed angle steel for rib-to-deck weld cracks was analyzed, with a focus on the influence of stiffener thickness, spacing, and arrangement on the reinforcement effect. Reasonable parameters were then suggested. The effectiveness of the proposed technology and parameters was demonstrated through a real bridge simulation. The results show that ribbed angle steel, compared to angle steel, offers effective reinforcement while being lighter in weight. The failure behaviour of ribbed angle steel is consistent with that of plain angle steel, and the quality of adhesive layer construction should be strictly controlled during actual implementation. Increasing the thickness of the stiffeners can enhance the reinforcement effect, while increasing the spacing between stiffeners can reduce the reinforcement effect. When using ribbed angle steel with 4 mm thick angle steel, 6 mm thick stiffeners, and 20 mm stiffener spacing to reinforce cracks, the reinforcement effect is superior to that of 10 mm plain angle steel.

Keywords: crack reinforcement technology; orthotropic steel deck; parameter analysis; rib-to-deck weld crack; ribbed angle steel

1. Introduction

Orthotropic steel decks (OSDs) are widely used in steel bridge construction due to their lightweight properties and superior load-bearing capabilities (Fisher and Barsom 2016, Yang *et al*. 2021). However, fatigue cracking in OSDs under prolonged vehicle loads has been increasingly observed worldwide, emerging as a primary concern affecting their performance and safety (Ahmadivala *et al.* 2021, Wang *et al*. 2015, Zhu *et al*. 2020). The rib-to-deck weld is a typical fatigue-prone detail in OSDs, with cracks initiating at the weld toe and propagating through the deck thickness being particularly hazardous (Zhu *et al*. 2022). Once these cracks penetrate the deck, they may result in secondary issues such as water leakage and corrosion, which can severely compromise bridge safety (Ya *et al*. 2011). Thus, effective methods are needed to treat these cracks promptly.

Several technologies have been developed to treat rib-to-deck weld toe (RDWT) cracks, including hole drilling, rewelding, UHPC pavement reinforcement, and local reinforcement. Among these, hole drilling will damage the deck and lead to water leakage, rendering it primarily a short-term solution (Okura and Ishikawa 2002). Rewelding is effective in preventing crack propagation, but it requires traffic interruption (Fu *et al*. 2017). UHPC pavement reinforcement can improve the overall stiffness of OSDs, thereby reducing the risk of cracking in the RDWs and inhibiting the propagation of existing cracks. However, the floorbeam cracks may still be a problem (Abdelbaset and Zhu 2024). Local reinforcement, which involves installing reinforcing components at cracked areas to increase local stiffness and inhibit crack propagation, has become the preferred method due to its advantages of avoiding traffic disruption and being convenient to implement (Abeln *et al*. 2022).

Current local reinforcement technologies include angle steel reinforcement, Fe-SMA reinforcement, and FRP reinforcement (Alemdar *et al*. 2014, Russian *et al*. 2022, Ke *et al*. 2021). Fe-SMA reinforcement applies compressive stress to the base material to inhibit crack propagation, with plate-shaped Fe-SMA currently used to reinforce diaphragm-rib weld cracks in OSDs (Qiang *et al*. 2023). However, the prestressing application and reinforcement effect of angle-shaped Fe-SMA require further investigation. FRP reinforcement mainly includes CFRP and GFRP. Liu *et al*. (2018) and Guo *et al*. (2019) have proven its effectiveness in reinforcing RDWT cracks through fatigue tests and short-term field monitoring, but noted that quality control during actual construction is difficult (Deng *et al*. 2023), which limits its use in real bridges. Angle steel reinforcement, which involves bonding L-shaped steel plates at cracked areas, is the main reinforcement method used in real bridges due to its low cost, ease of installation, and non-destructive nature (Zhou and Xu 2021, Jiang *et al*. 2024). However, in real bridges, the angle steel is typically installed in an "inverted" state,

*Corresponding author, Professor
E-mail: fuzhongqiu@hhu.edu.cn

ISSN: 1229-9367 (Print), 1598-6233 (Online)

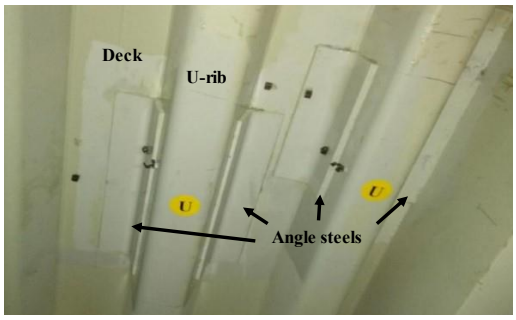

Fig. 1 Angle steel reinforcement in real bridge

with the adhesive layer bearing the full weight. Long-term heavy-duty service conditions accelerate the cracking of the adhesive layer, and research indicates that once the adhesive layer cracks, the reinforcement effect significantly diminishes (Al-Mosawe *et al*. 2024). Therefore, minimizing the self-weight of the reinforcing component when bonding angle steel is crucial to avoid exacerbating adhesive layer deterioration, but this inevitably reduces the reinforcing effect of the angle steel itself.

Moreover, as the service life of OSDs increases, fatigue cracking at rib-to-deck welds is becoming more severe, with multiple cracks appearing in single compartments. Field inspections of a kilometer-class cable-stayed bridge in China revealed multiple rib-to-deck cracks concentrated in a single compartment, which were reinforced with angle steel, as shown in Fig. 1. Multiple reinforcements in a single compartment inevitably lead to increased local weight, potentially affecting the overall stress of the bridge. Hence, efficient, lightweight, and convenient reinforcement technologies are essential for future bridge maintenance. To address this, some scholars have proposed the corner brace reinforcement technology, which involves welding corner braces at rib-to-deck welds. This technology effectively limits local deformation and crack propagation but introduces secondary cracking issues at the welded connections (Fu *et al*. 2018, Li 2018). To overcome the limitations of existing reinforcement technologies and meet the need for efficient, lightweight, and convenient reinforcement technologies for treating multiple cracks in OSDs, a high-efficiency lightweight reinforcement technology using ribbed angle steel (RAS reinforcement technology) was proposed. Ribbed angle steel, cast integrally using molds, consists of thin-walled angle steel and stiffeners. The incorporation of stiffeners compensates for the loss of stiffness due to the reduced thickness of the angle steel while reducing the self-weight of the reinforcing component. This approach also avoids secondary cracking problem caused by directly welding corner braces to the deck.

In this paper, reinforcement tests and numerical simulations were conducted, the effectiveness of RAS reinforcement in treating RDWT cracks was evaluated. The impacts of parameters such as stiffener thickness, arrangement, and spacing on the reinforcement effect were discussed. Based on the analysis results, practical parameters for bridge applications were recommended, and the effectiveness of the proposed technology and parameters was demonstrated through real bridge simulations.

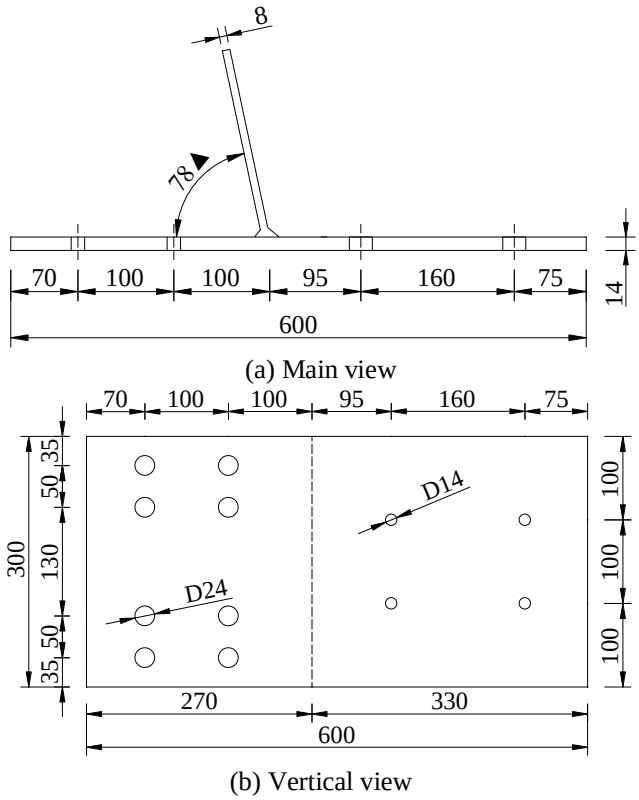

Fig. 2 Size of the specimen

2. Reinforcement test

2.1 Specimen design

Considering the manufacturing and testing costs, the local full-scale specimen of the rib-to-deck weld was designed based on the dimensions of the real bridge, as shown in Fig. 2. In the specimen, the deck dimensions are 600 mm × 300 mm × 14 mm, and the U-rib dimensions are 300 mm × 200 mm × 8 mm. The angle between the U-rib and the deck is 78°, with the connection being achieved through double-sided welding. The size of the weld toe on the outer side is 10 mm, while the size of the weld toe on the inner side is 8 mm. All specimens are made of Q345qD steel used in the real bridge.

2.2 RAS design and test conditions

The RAS is comprised of an angle steel and stiffeners, as shown in Fig. 3. Initially, it was planned to integrate the two components through casting. However, considering the limited number of RAS components used in this test and the high cost of mold production, spot welding was employed to connect them. In the test, six RASs of different dimensions and one plain angle steel were designed, and a total of seven test conditions, numbered SJ1 to SJ7. Among these, SJ1 to SJ3 were used to analyze the influence of the

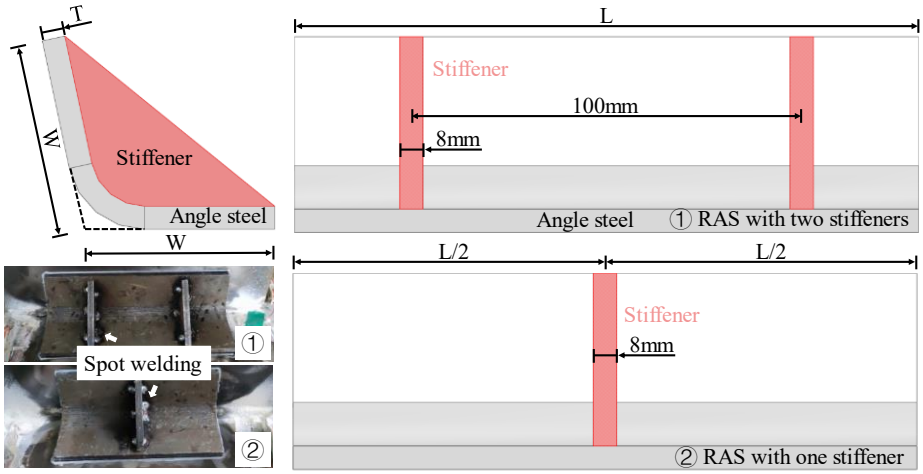

Fig. 3 Schematic diagram and physical diagram of the RAS

Table 1 Test conditions

Specimen	Parameters of RAS				
	Length of the angle steel L (mm)	Thickness of the angle steel T (mm)	Width of the angle steel W (mm)	Thickness of the stiffener (mm)	Number of the stiffener
SJ1	160	6			0
SJ2	160	6			1
SJ3	160	6			2
SJ4	120	6	50	8	2
SJ5	200	6			2
SJ6	160	4			2
SJ7	160	8			2

Table 2 Mechanical properties and chemical composition of Q345qD

Yield strength (MPa)	Tensile strength (MPa)	Elongation (%)	Chemical composition (%)				
			C	Si	Mn	P	S
385	540	31.5	0.14	0.31	1.46	0.016	0.006

Table 3 Material properties of the adhesive

Material properties	Tensile strength (MPa)	Elastic modulus (MPa)	Poisson's ratio	Elongation (%)	Heat distortion temperature (℃)
Measured indicators	44.2	5596	0.26	1.26	69.5

number of stiffeners. For configuration with a single stiffener, it was placed at the center of the angle steel. When two stiffeners were set, they were symmetrically arranged 100 mm apart on either side of the angle steel, as detailed in Fig. 3. SJ3 to SJ5 were used to analyze the influence of the angle steel's length, and SJ3, SJ6, and SJ7 were used to analyze the influence of the angle steel's thickness. In all conditions, the width (W) of the angle steel was uniformly set to 50 mm, and the thickness of the stiffeners was set to 8 mm. The specific test conditions are shown in Table 1.

2.3 Material properties

The steel materials used for the specimens and RASs is Q345qD. The corresponding Young's modulus and Poisson's ratio are 206 GPa and 0.3, respectively, and the mechanical properties and chemical composition of the steel are shown in Table 2. The adhesive used is a room temperature curing type A-grade structural adhesive, whose material performance indicators comply with the "Design Code for Highway Bridge Reinforcement" (JTG/T J22-2008). The main properties are shown in Table 3.

2.4 Test procedure and reinforcement conditions

The test is comprised of two stages: Stage 1, the crack pre-fabrication stage, and Stage 2, the reinforcement test stage, as shown in Fig. 4.

Stage 1: Fix the specimen onto the steel base using high-strength bolts. Subsequently, the reinforcement areas are marked, and the coating within these areas is removed using a grinder. After grinding, uniaxial strain gauges are affixed

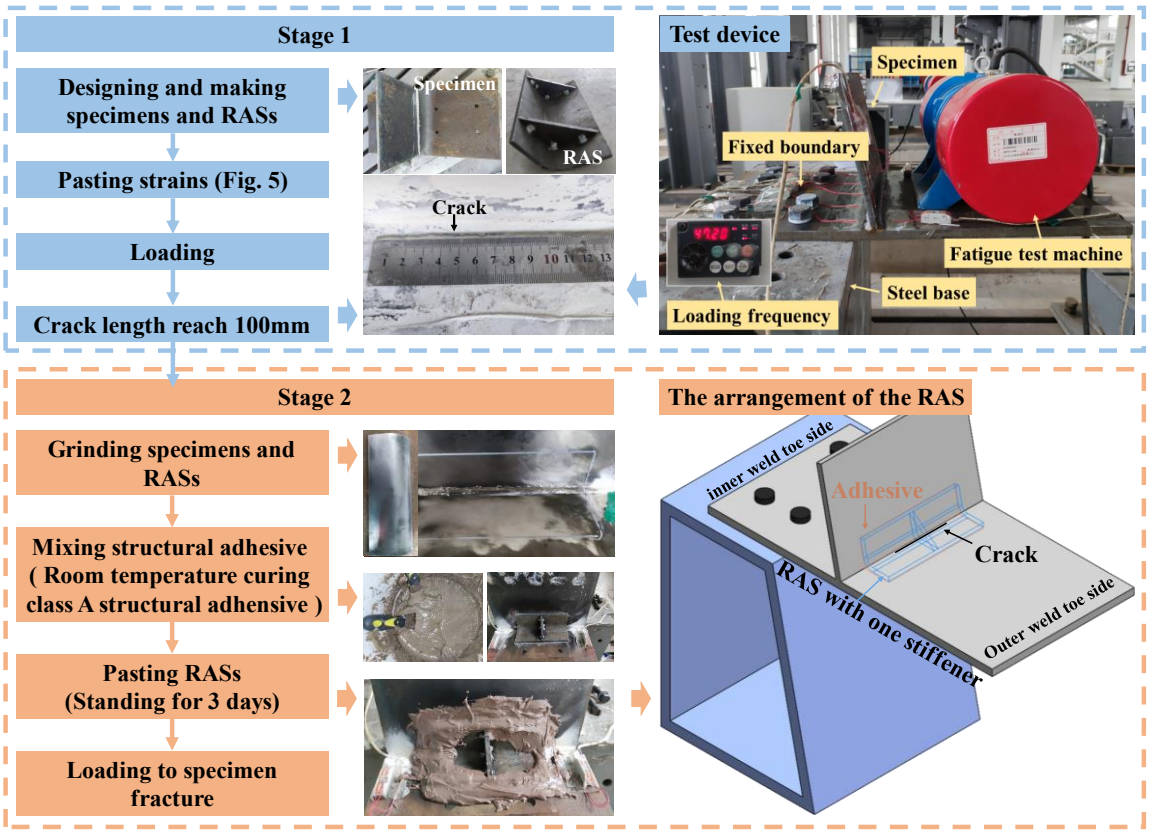

Fig. 4 Testing procedures

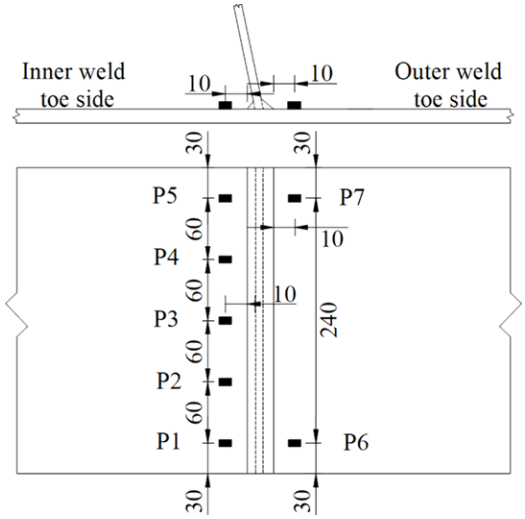

Fig. 5 Layout of measured points (unit: mm)

at 10 mm from both the inner and outer weld toes (numbered P1 to P7). The longitudinal direction of the strain gauges is perpendicular to the weld, and the spacing along the width direction of the specimen is shown in Fig. 5. Following the attachment of the strain gauges, cyclic loading is applied by the fatigue testing machine on the deck at the outer weld toe side, as shown in Fig. 4. The loading frequency is set to 47.2 Hz with a stress ratio of -1. The strain amplitude measured at point P3 is controlled to be 720 $\mu\varepsilon$ by adjusting the angle of the eccentric block in the fatigue testing machine. This stage ends when the crack propagates to 100 mm.

Stage 2: Upon the crack propagating to 100 mm, the fatigue testing machine is removed while the strain gauges are retained. The RASs are then bonded to the cracked area using structural adhesive, ensuring the midline of the angle steel in the longitudinal direction coincides with the center of the crack. The adhesive layer thickness is controlled between 2 to 3 mm. Following the bonding of RASs, a curing period of 3 days is required before reloading. Subsequently, the specimen is reloaded with the same loading frequency and magnitude as in Stage 1 until the

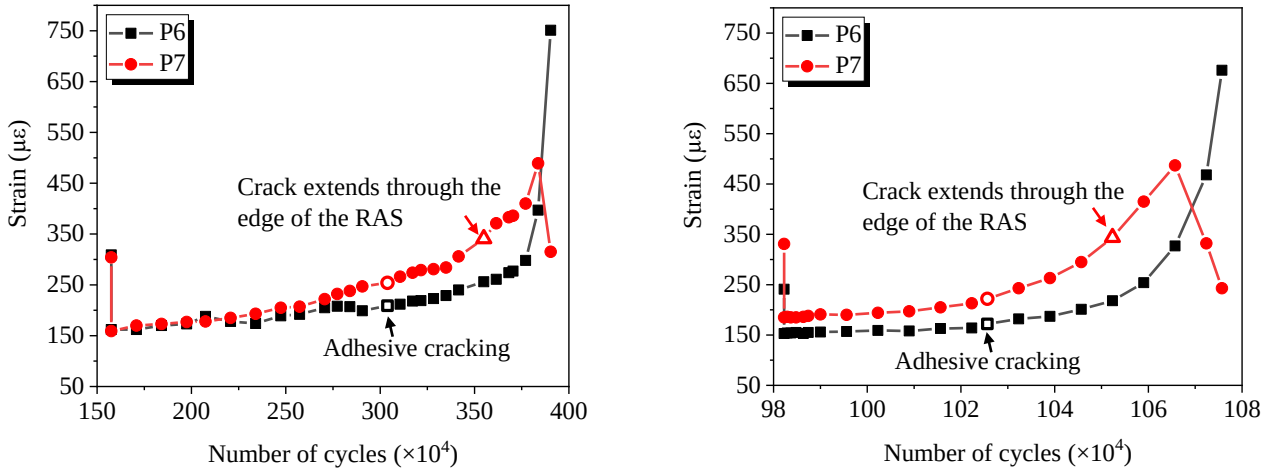

Fig. 6 Strain time history curve of measurement points at the outer weld toe

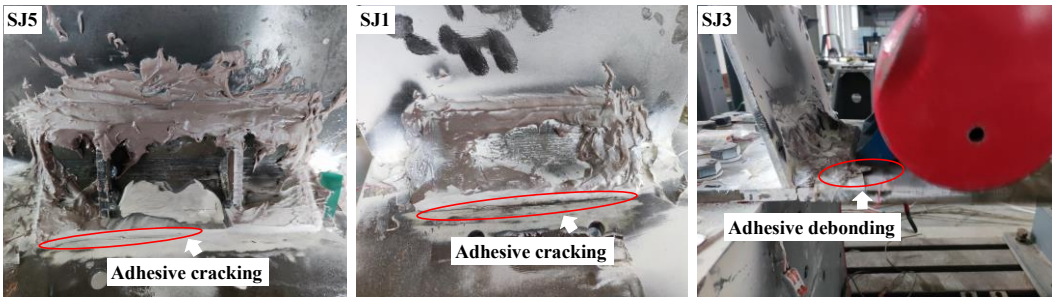

Fig. 7 Adhesive failure

specimen fractures.

3. Analysis of test results

3.1 Local stress

Taking SJ5 and SJ7 as examples, the strain time-history curves for each measurement point at the outer weld toe after reinforcement are shown in Figs. 6(a)-6(b). From the Figure, it can be observed that after being reinforced with RAS, the strains at each measurement point of SJ5 and SJ7 have decreased by approximately 47.6%, 47.7%, 36.5%, and 44.1% respectively. Notably, there is a certain difference in the strain reduction at the two measurement points of SJ7, which is considered to be due to asymmetric crack propagation. It is evident that using RAS to reinforce RDWT cracks can effectively reduce the local deformation of the component and suppress crack propagation.

Based on the observations during the test process and the strain time-history curves of the measurement points, it can be noted that when structural adhesive is used to bond RAS, the entire failure process of the reinforcement primarily exhibits the following stages: initially, the adhesive layer at the edge of the RAS cracks (as shown in Fig. 7, SJ5), followed by a gradual increase in local strain. Subsequently, continuous enlargement of the adhesive cracks occurs, and the cracks rapidly propagate to the edge of the angle steel. Finally, approaching failure, the RAS is almost debonding from the deck (as shown in Fig. 7, SJ3), and the crack penetrates through the deck, leading to specimen fracture and failure. Taking SJ5 as an example, when the load is cyclically applied for 1,463,500 times after being reinforced with RAS, the adhesive layer at the edge of the RAS begin to crack, and the strain at the outer weld toe gradually increases. After applying an additional 510,000 cycles, the crack extend to the edge of the RAS on the P7 measurement point side, and the crack then rapidly propagate. After just 354,700 more cycles, the specimen fracture and fail. It is evident that once the adhesive layer cracks, the reinforcement effect of the RAS rapidly deteriorates, and the crack propagation rate increases. Furthermore, comparing SJ5, SJ3 (RAS) with SJ1 (plain angle steel) in Fig. 7, it can be observed that the failure process of RAS reinforcement is essentially consistent with that of plain angle steel.

From the above analysis, it can be concluded that RAS can improve the local stiffness of the rib-to-deck weld and inhibit crack propagation. However, its reinforcement effect is limited by the quality of the adhesive layer. Once the adhesive layer cracks, the reinforcement effect of the RAS will gradually weaken until it fails completely. Therefore, during practical bridge applications, strict control over adhesive layer construction quality is essential to ensure the reinforcement effect of the RAS. Moreover, immediate replacement should be carried out if adhesive layer cracking

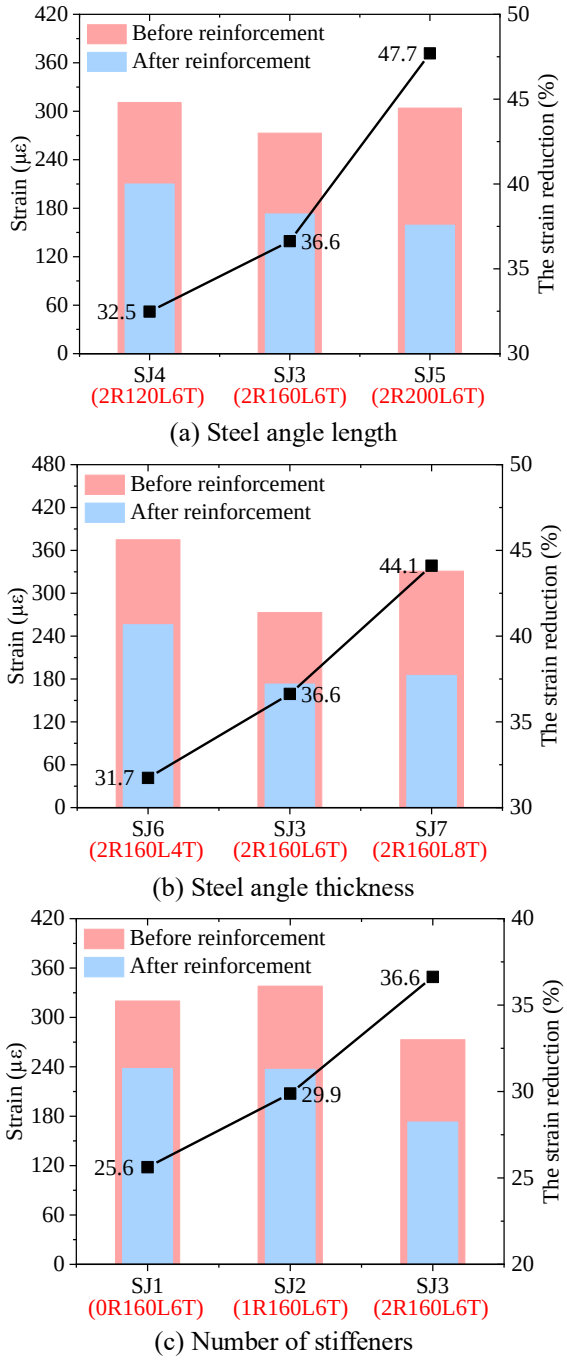

Fig. 8 Strain reduction at measurement points on each specimen

is detected.

3.2 Parameter impact analysis

The strain reduction at the P7 measurement points before and after reinforcement are plotted in Figs. 8(a)-8(c). From Fig. 8(a), it can be observed that when two stiffeners are arranged, the strain reduction increases with the length of the angle steel. The strain reduction for 160 mm long angle steel is 4.1% higher compared to 120 mm long angle steel, while 200 mm long angle steel shows an 11.1% higher strain reduction compared to 160 mm long angle

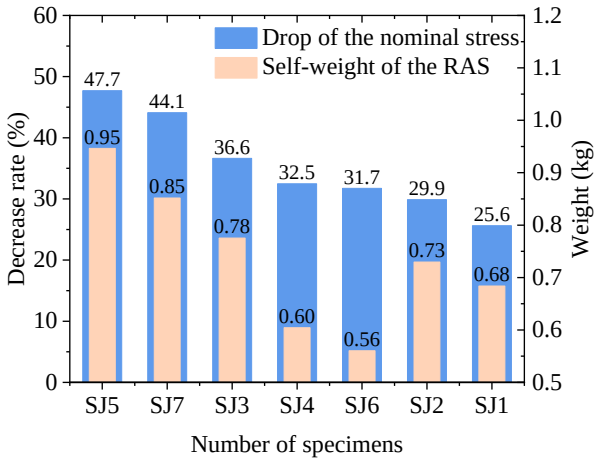

Fig. 9 Strain change and self-weight of each specimen

steel. This indicates that with the same number of stiffeners, increasing the length of the angle steel can enhance its reinforcement effect.

From Fig. 8(b), it is evident that when two stiffeners are arranged, the strain reduction increases with the thickness of the angle steel. The strain reduction for 6 mm thick angle steel is 4.9% higher compared to 4 mm thick angle steel, and 8 mm thick angle steel shows a 7.5% higher strain reduction compared to 6 mm thick angle steel. This suggests that with the same number of stiffeners, increasing the thickness of the angle steel can also improve its reinforcement effect.

From Fig. 8(c), it is evident that when one stiffener is used, the strain reduction at the measurement point is 4.3% higher compared to plain angle steel. When two stiffeners are arranged, the strain reduction increases to 36.6%, which is 11.0% higher compared to plain angle steel. This demonstrates that adding stiffeners can further enhance the reinforcement effect of the angle steel, as it increases its bending stiffness and restricts bending deformation, thus more effectively reducing deformation at the rib-to-deck weld.

To further validate the feasibility of the proposed technology, the strain reduction and self-weight of each specimen are plotted in descending order, as shown in Fig. 9. The self-weight (W) of the RAS is obtained through Eq. (1), where A_s is the cross-sectional area of the angle steel (mm^2), A_r is the cross-sectional area of the stiffener (mm^2), both of which are calculated using CAD software. L is the length of the angle steel (mm), T is the thickness of the stiffener (mm), N is the number of the stiffener, and ρ is the density of the steel, which is 7.85×10^{-6} kg/mm^3. Comparing SJ1 and SJ6, it is found that the strain reduction for 160 mm long, 4 mm thick angle steel with two stiffeners is approximately 6.1% greater than for 160 mm long, 6 mm thick plain angle steel, and its weight is also lighter, reduced by about 17.6%. Comparing SJ4 and SJ1, it is observed that the strain reduction for 120 mm long, 6 mm thick angle steel with two stiffeners is approximately 6.9% greater than for 160 mm long, 6 mm thick pure angle steel, and its weight is reduced by about 11.8%. These findings demonstrate that the RAS reinforcement technology

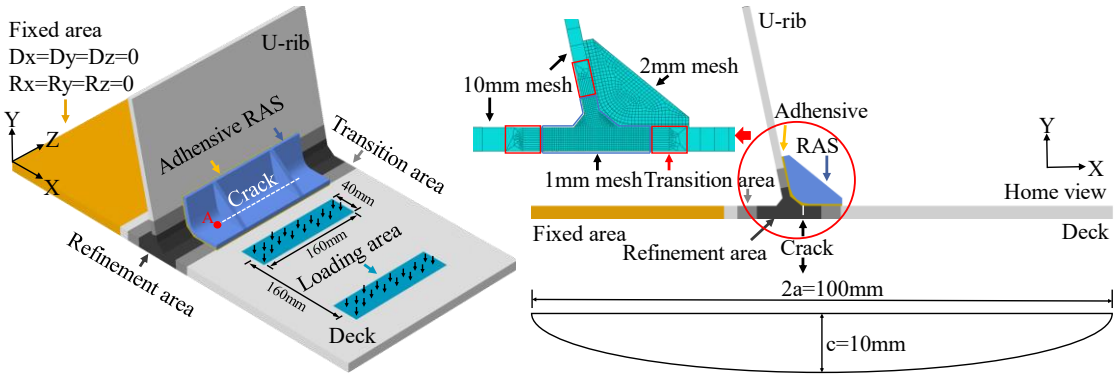

Fig. 10 Finite element model

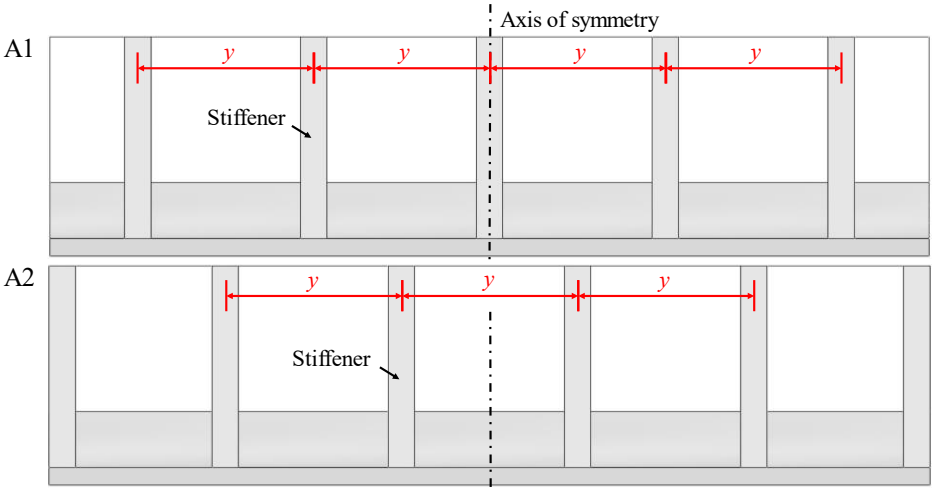

Fig. 11 Arrangement form of stiffeners (A1/A2)

proposed in this paper can reduce the additional weight introduced while ensuring the crack reinforcement effect, an effective method for reinforcing multiple cracks within a single compartment.

$$W=(A_sL+A_rTN)\rho \quad (1)$$

4. Numerical simulation

4.1 Finite-element model

Considering the premature failure of the adhesive layer during the test, a numerical simulation was performed to further discuss the influence of RAS parameters on the reinforcement effect. ABAQUS finite element analysis software was used to establish models of cracked rib-to-deck weld specimens and RAS, as shown in Fig. 10. The dimensions of the specimen model are consistent with the actual specimen in the test. The elastic modulus of both the specimen and RAS is 2.06×10^5 MPa, with a Poisson's ratio of 0.3. The adhesive layer has an elastic modulus of 5,596 MPa and a Poisson's ratio of 0.26, with a thickness of 2mm. The "Tie-connection" was employed to simulate the adhesive connection between the specimen, RAS, and adhesive layer.

A fixed constraints, constraining all translational and rotational degrees of freedom, was applied to the inner weld toe side of the deck in the specimen model. A uniformly distributed load was applied to the deck on the outer weld toe side, consistent with the test loading position. The loading area corresponded to the actual contact area between the fatigue testing machine and the specimen, measuring 160 mm × 40 mm, with a center-to-center distance of 160 mm between the two loading surfaces. In the simulation, static loading was applied, controlling the X-direction normal stress at point P3 in the model to be half of the stress amplitude in the test. Taking SJ2 as an example, this translated to a surface load of 0.30 MPa in the model.

The model was constructed using solid elements and meshed with C3D8R hexahedral elements. The global mesh size is 10 mm, with 1 mm mesh refinement applied to the deck plate within 20 mm of the outer and inner weld toes, and within 10 mm of the U-rib area near the weld toe. The refined area transitions to other regions using two layers of hexahedral swept mesh. The RAS and adhesive layer is refined with 2 mm mesh.

In the model, the crack was simplified to a semi-elliptical shape, with the long semi-axis length c set to 50 mm and the short semi-axis length a set to 10 mm. In the X direction, the crack is 0.5 mm from the outer weld toe of the specimen, whilst in the Z direction, the crack center aligns

Table 4 Simulation conditions

Reinforcement condition	Angle steel length a (mm)	Angle steel thickness x (mm)	Spacing of stiffeners y (mm)	Thickness of stiffeners (mm)	Stiffener arrangement
160L10T0R	160	10	/	/	/
200L10T0R	200	10			
160L4T0R	160	4			
200L4T0R	200	4			
160LxT100R-A2	160	4/6	100	2-12 (Average 2)	A2
200LxT100R-A2	200				
160LxTyR-A1	160	4/6	20-80 (Average 10)	6	A1/A2
160LxTyR-A2					
160LxTyR-A2			90, 120-160 (Average 20)		A2
200LxTyR-A1	200	4/6	20-90 (Average 10)	6	A1/A2
200LxTyR-A2					
200LxTyR-A2			120-200 (Average 20)		A2

Table 5 ominal stress at measured points in simulation and test

Measured points	P1	P2	P4	P5	P6
Test (MPa)	67.1	72.4	77.0	75.8	68.5
Simulation (MPa)	69.8	74.9	77.0	74.9	69.8
Error (%)	4.0	3.5	0	1.0	2.0

with the specimen center. The XFEM function in ABAQUS was used to calculate the stress intensity factors at the crack tip under different reinforcement conditions (Fang *et al*. 2023).

4.2 Parameters of the stiffener

Field investigations of bridge repair strategies in China have revealed that 10 mm thick plain angle steel is widely used for reinforcing RDWT cracks. Based on this prevalent practice, two types of RASs with angle steel thicknesses of 4mm and 6mm, lengths of 160mm and 200mm, and a width of 50mm are considered in this paper. The design parameters for stiffener thickness, arrangement, and spacing are presented in Table 4. The name for each reinforcement condition is derived from the angle steel's dimensions and stiffener characteristics. The influence of stiffener thickness on reinforcement efficacy is analyzed under conditions 160LxT100R-A2 and 200LxT100R-A2. Based on the results (discussed in section 4.4.1), 6mm thick stiffeners are selected, and the effects of stiffener arrangement (A1 and A2) and spacing are analyzed subsequently. In A1, stiffeners are symmetrically arranged along the central axis of the angle steel, with equal spacing towards both sides. In A2, stiffeners are symmetrically arranged from the center outward. The specific arrangements are shown in Fig. 11.

4.3 Validity verification

Taking SJ2 as an example, the stresses measured at various points along the inner weld toe during initial loading are compared with finite element simulation results, as presented in Table 5. The errors between the test and simulation at each measuring point are within 5%. The close agreement between experimental and simulated results validates the model's reliability for subsequent analysis.

4.4 Influence analysis of stiffener parameters

The Stress Intensity Factor (SIF) is widely used to predict the stress state near crack tip and serves as a crucial parameter for evaluating crack propagation behavior (Wang *et al*. 2019, Oda *et al*. 2024). In fracture mechanics, cracks are classified into three modes: opening mode (tensile stress perpendicular to the crack surface), sliding mode (shear stress parallel to the crack propagation direction), and tearing mode (shear stress perpendicular to the crack propagation direction). These modes are characterized by stress intensity factors K_{I}, K_{II}, and K_{III}, respectively, which describe the stress field near the crack tip for each mode (Merzoug *et al*. 2017). Compared to local stress, SIF more accurately reflects the crack propagation capability after reinforcement. Previous research has demonstrated that under bending loads, the crack tip at the rib-to-deck weld is primarily governed by K_{I} (Wang *et al*. 2021). Consequently, the impact of RAS parameters on crack reinforcement effectiveness is assessed the K_{I} at the crack tip.

4.4.1 Stiffener thickness

Using the 200LxT100R-A2 and 160LxT100R-A2 conditions as examples, the K_{I} at the crack tip under different stiffener thicknesses is extracted, as shown in Fig. 12. The data reveal that when using plain angle steel, the K_{I} at the crack tip gradually decreases as the length and thickness of the plain angle steel increase. Notably, the

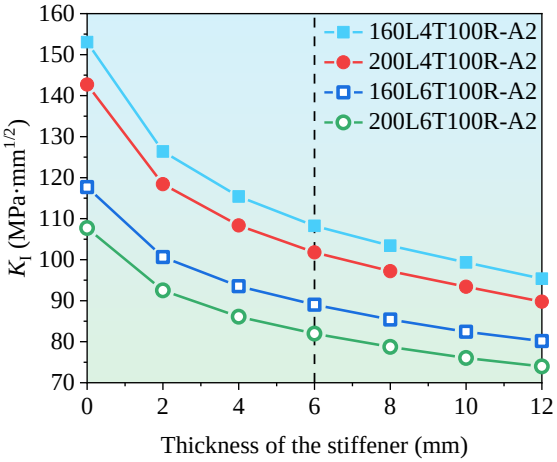

Fig. 12 The K_I at crack tip under the reinforcement condition of 200L*x*T100R-A2 and 160L*x*T100R-A2

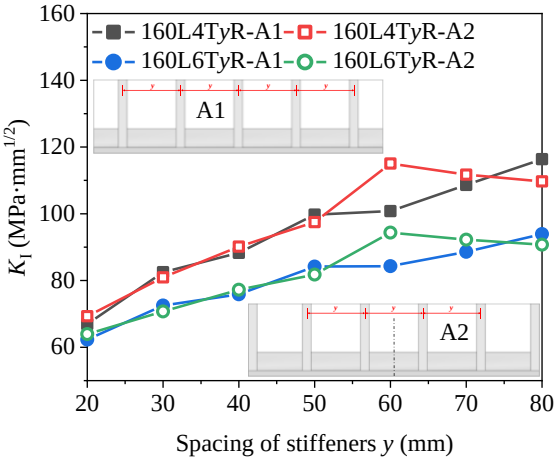

(a) 160L

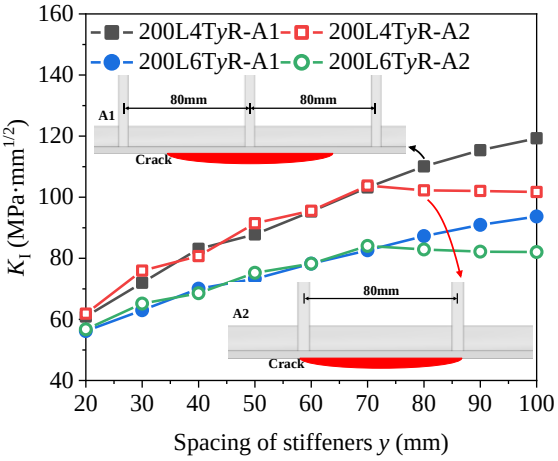

(b) 200L

Fig. 13 The K_I at crack tip under different reinforcement condition

increment in plain angle steel thickness demonstrates a more pronounced effect on enhancing reinforcement effect compared to increasing the angle steel length.

Upon setting stiffeners, the K_I at the crack tip gradually decreases as the stiffener thickness increases. This trend remains consistent across different angle steel lengths and thicknesses. When the stiffener thickness is 6mm, the K_I decreases by 29.3%, 28.7%, 24.4%, and 23.9% respectively compared to the case without stiffeners. Subsequently, for every additional 2 mm in stiffener thickness, the reduction in K_I decreases gradually, with the decrease remaining within 5%. It can be seen that when the stiffener thickness is greater than 6mm, increasing the stiffener thickness has limited improvement on the reinforcement effect of the RAS. Considering that increasing the stiffener thickness will further increase the self-weight of the RAS, and that the reinforcement effect of RAS can also be improved by changing parameters such as stiffener arrangement and spacing, a 6mm stiffener is recommended.

4.4.2 Stiffener arrangement

By comparing the number of stiffeners under the A1 and A2 arrangement forms, it is observed that when the length of the angle steel is 160 mm with stiffener spacing $y \leq 80$mm, or 200mm with $y \leq 100$mm, the two arrangement forms differ in stiffener positions and numbers. Thus, the K_I at the crack tip are calculated under the condition within the above conditions to investigate the impact of stiffener arrangement on reinforcement effect, as shown in Figs. 13(a)-13(b).

For RAS with 160mm long angle steel, when $y \leq 50$mm, the differences in K_I between the two arrangement forms are small (<4%), when $y > 50$mm, the K_I increases with stiffener spacing in A1, while it decreases in A2. For RAS with 200mm long angle steel, when $y \leq 70$ mm, the K_I differences are small (<6%), when $y > 70$ mm, the K_I increases with stiffener spacing in A1 but slowly decreases in A2. Evidently, for varying angle steel lengths and thicknesses, the A1 arrangement shows a diminishing reinforcement effect with increased stiffener spacing, while A2 initially decreases then increases.

Furthermore, by comparing the position and number of stiffeners in the K_I descending section in Fig. 13, it can be found that A1 consistently has 3 stiffeners, with non-central stiffeners moving farther from the crack tip as spacing increases. A2 has 2 stiffeners, moving closer to the crack tip with increased spacing. For instance, with 200mm angle steel and 100mm spacing (stiffeners directly above the crack tip), the K_I reduction at the crack tip is maximized. This suggests that positioning stiffeners at the crack tip can further enhance the local stiffness, reduce the stress intensity factor at the crack tip, and improve the reinforcement effect of the RAS. Considering that A2 generally requires fewer stiffeners than A1 while providing comparable or superior reinforcement, it is recommended for practical bridge applications.

4.4.3 Stiffener spacing

Based on the above analysis, the K_I at the crack tip and the self-weight of the RAS after reinforcement are calculated, using the 200LxTyR-A2 reinforcement condition as an example (Figs. 14(a)-14(b)). The results reveal that for angle steels of varying thicknesses, the K_I exhibits a non-monotonic trend as the spacing of stiffeners increases, initially rising, then declining, before increasing

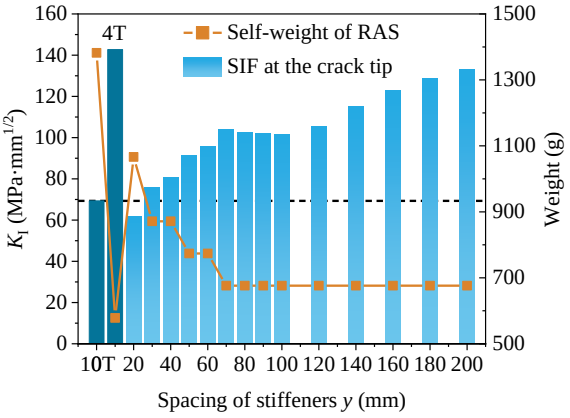

(a) x=4mm

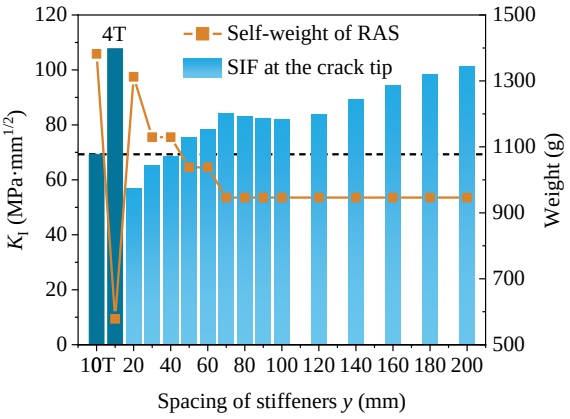

(b) x=6mm

Fig. 14 The K_I at crack tip under the reinforcement condition of 200LxTyR-A2

again. Notably, the self-weight of RASs, regardless of thickness and stiffener spacing, remains consistently lower than that of a 10 mm thick plain angle steel.

For RAS with 4mm thick angle steel and 20mm stiffener spacing, the K_I is approximately 10.7% lower than that of 10mm thick plain angle steel, and the self-weight of the RAS is reduced by 22.8%. For RAS with 6mm thick angle steel and stiffener spacing y≤40mm, both the K_I and the self-weight are less than those of 10mm thick plain angle steel. At 40mm spacing, the K_I is virtually equivalent to that of 10mm thick plain angle steel (less than 1.2%), while the RAS self-weight is reduced by approximately 18.3%. When the spacing is reduced to 20mm, the K_I at the crack tip decreases by about 18.1% compared to 10mm thick plain angle steel, with only a 5.0% reduction in RAS self-weight. Whilst this configuration demonstrates superior reinforcement efficacy compared to RAS with 4mm thick and 20mm stiffener spacing, it offers less reduction in self-weight.

Given that both options yield K_I values post-reinforcement lower than that of 10mm thick plain angle steel, it is recommended to employ RAS with 4mm thick angle steel and 20mm stiffener spacing for reinforcing the RDWT cracks in practical bridge applications. This configuration ensures effective reinforcement while minimising the additional self-weight of the reinforcement structure as much as possible.

5. Real bridge simulation verification

5.1 Finite-Element Model

To further validate the feasibility and effectiveness of the proposed technology and its parameters in practical bridge applications, a OSD segment model was established using the finite element analysis software ABAQUS, based on the actual dimensions of a kilometer-level cable-stayed bridge in China, as shown in Fig. 15. The segment model spans seven U-ribs transversely, with each rib having an opening width of 300 mm, a height of 300 mm, a thickness of 8 mm, and a spacing of 600 mm, sequentially numbered U1 to U7. Longitudinally, the model includes five diaphragms with a height of 1,000 mm and a thickness of 10 mm, sequentially numbered D1 to D5, and a deck thickness of 14 mm. The model employs solid elements and was meshed with C3D8R hexahedral elements of 50 mm. The material properties are consistent with Q345qD steel, with an elastic modulus of 2.06×10^5 MPa and a Poisson's ratio of 0.3. Constrain all translational degrees of freedom for the deck plate and U-ribs in the segmental model, and constrain both translational and rotational degrees of freedom for the diaphragms.

To enhance calculation accuracy and efficiency, a sub-model measuring 500 mm in length and 600 mm in width was extracted from the segment model. The sub-model is transversely located at the fourth U-rib and longitudinally between diaphragms D3 and D4, and is connected to the segment model using the 'Submodel' technique in the software. The submodel shares the same element type and material properties as the segment model. For the deck 20 mm from the weld toe and weld root and the U-rib 10 mm from the weld toe, the mesh is refined with 2 mm C3D8R hexahedral elements, and other regions are meshed with 10 mm elements. The refined and coarser mesh regions transition using two layers of swept hexahedral elements.

Both the segment model and the submodel are configured with a through-crack of 200 mm in length, simplified to a rectangular shape. Longitudinally, the crack is centered between diaphragms D3 and D4. Transversely, it is positioned to the right of the fourth U-rib, 0.2 mm from the weld toe. The XFEM function in ABAQUS was used to calculate the stress intensity factors at the crack tip under different reinforcement conditions.

Based on the parameters proposed in the paper, two reinforcement conditions, 300L10T0R and 300L4T20R-A2, are implemented in both the segment model and sub-model. A 2mm adhesive layer is set between the RAS and the segment model and sub-model, connected using 'Tie connection'. The RAS is assigned the same material properties as the segment model, while the adhesive layer properties are consistent with those described in section 4.1. In the segment model, the RAS and adhesive layer are meshed with 5 mm elements, while in the sub-model, 2 mm elements are used.

The fatigue load model III from the JTG D64 (2015) standard is employed, applying a single-sided double wheel load. Considering the load dispersing effect of the pavement, the load area is set to 300 mm × 700 mm

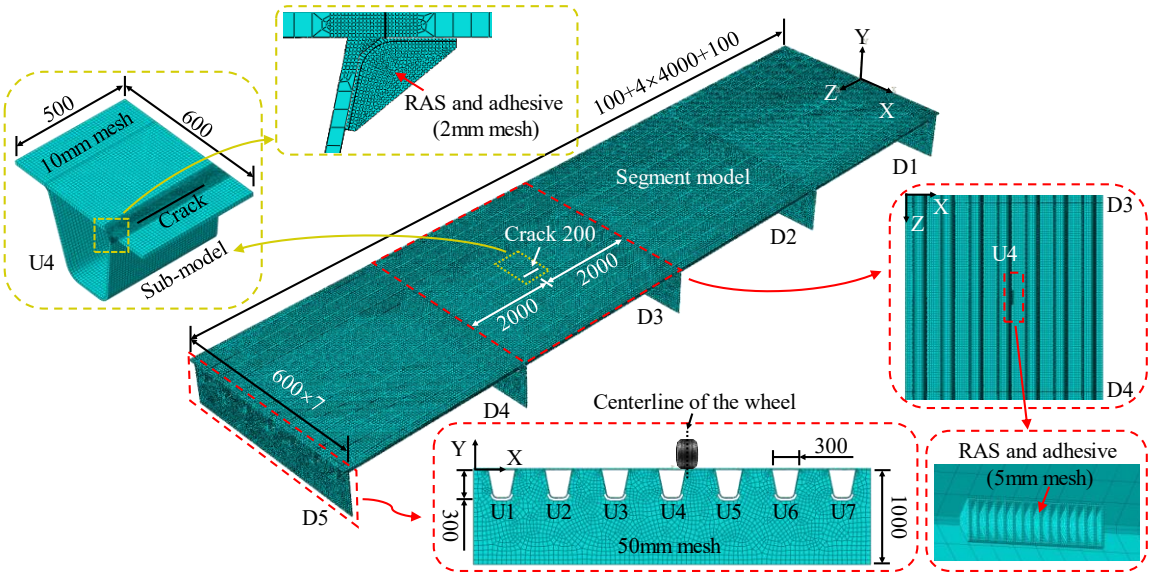

Fig. 15 Segment model (unit: mm)

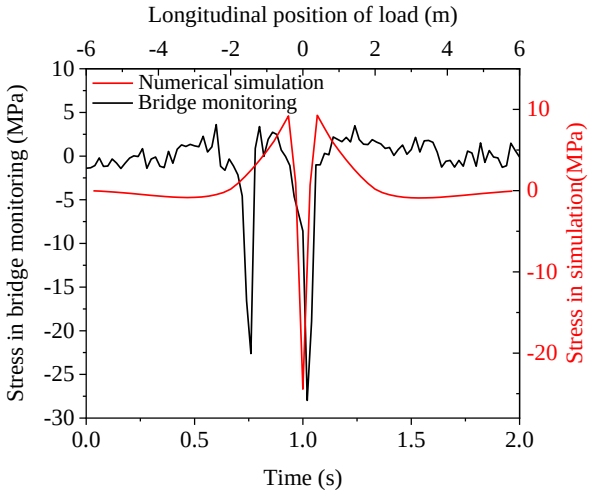

Fig. 16 Stress in simulation and bridge monitoring

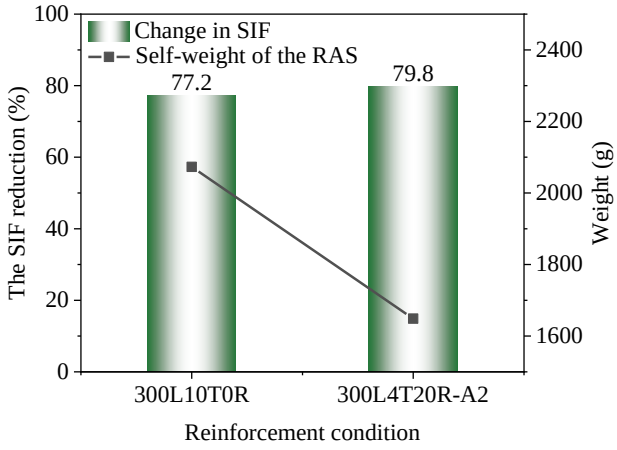

Fig. 17 The SIF reduction at crack tip and the self-weight of the RAS

(longitudinal × transverse), with a single-sided axle weight of 60 kN, equivalent to a load intensity of 0.29 MPa. Transversely, the load center is positioned directly above the cracked weld. Longitudinally, the load is moved from the D2 to D5 diaphragm in 200 mm increments.

5.2 Validity verification

To verify the effectiveness of the model, stress monitoring was conducted to obtain the stress time history curves of the rib-to-deck weld under vehicle load in the real bridge. The monitoring results were compared with the model calculation results. The monitoring points on the actual bridge were consistent with the positions in the submodel. Single-direction strain gauges were attached 10mm away from the weld toe on the deck, and a uT78 static and dynamic strain meter was used to monitor the strain of the gauges. The strain was converted to stress based on Eq. (2), where σ is the stress (MPa), E is the elastic modulus of the steel (MPa), and ε is the measured strain.

A stress time history curve was extracted when a two-axle vehicle passed during the monitoring process and compared with the simulation results, as shown in Fig. 16. The Figure shows that the variation patterns of the two stress curves obtained from the real bridge monitoring and simulation are basically consistent, with only some differences in stress magnitude. It can be concluded that the model is reasonable and can be used for subsequent research.

$$\sigma = E\varepsilon \tag{2}$$

5.3 Effect evaluation

The SIF reduction at the crack tip after reinforcement compared to the unreinforced state and the self-weight of the RAS were calculated for each condition, as shown in Fig. 17. The Figure indicates that RAS reinforcement achieves slightly higher SIF reduction at the crack tip compared to plain angle steel, while reducing self-weight

by 20.5%. This demonstrates that the proposed RAS reinforcement technology and recommended parameters are feasible and effective. In actual bridges, it can replace current plain angle steel reinforcement methods, ensuring reinforcement effectiveness while reducing the local weight introduced to the bridge.

6. Conclusions

In this papar, a high-efficiency lightweight reinforcement technology using RAS was proposed. The effect of RAS reinforcement on the RDWT cracks was analyzed by conducting reinforcement tests and numerical simulations. The influence of parameters such as stiffener thickness, spacing, and arrangement on the reinforcement effect was discussed, and reasonable parameters were suggested. The conclusions are as follows:

• Compared to plain angle steel and corner brace reinforcement, the proposed RAS reinforcement technology involves setting stiffeners on thin-walled angle steel, which avoids the secondary cracking problem caused by corner brace reinforcement and can achieve better crack reinforcement effects while having lighter self-weight, providing a new technology for treating RDWT cracks in actual bridges.

• Increasing the thickness of stiffeners in RAS can improve its reinforcement effect. When the stiffener thickness is greater than 6 mm, further increase has limited improvement on the reinforcement effect. It is recommended to use 6 mm thick stiffeners for real bridges.

• The RAS with 4 mm thick angle steel and stiffeners arranged symmetrically at 20 mm intervals from the angle steel's symmetry axis has better reinforcement effect and lighter self-weight compared to 10 mm thick plain angle steel. It is recommended to refer to these parameters for real bridge reinforcement.

• The failure behavior of bonded RAS is basically consistent with that of plain angle steel, mainly manifested as the adhesive layer cracking first, gradually losing the reinforcement effect, and finally completely debonding. Strict control of adhesive layer construction quality should be implemented in real bridge reinforcement, and the adhesive layer should be replaced once cracking is detected.

• Real bridge simulation results show that the RAS parameters proposed in this paper meet the application requirements of actual bridges. According to the parameters proposed in this paper, it can be pre-cast in the factory using molds and then cut according to the crack length during actual bridge reinforcement.

Acknowledgments

The research is supported by the National Natural Science Foundation of China (No. 52378153) and Postgraduate Research & Practice Innovation Program of Jiangsu Province (No. KYCX24_0852). The assistance is gratefully acknowledged.

References

Abeln, B., Gessler, A., Stammen, E., Ilg, F., Feldmann, M., Dilger, K. and Schuler, C. (2022), "Strengthening of fatigue cracks in steel bridges by means of adhesively bonded steel patches", *J. Adhes.*, **98**(6), 827-853. https://doi.org/10.1080/00218464.2021.2006059.

Abdelbaset, H. and Zhu, Z.W. (2024), "Behavior and fatigue life assessment of orthotropic steel decks: A state-of-the-art-review", *Structures.*, **60**, 105957. https://doi.org/10.1016/j.istruc.2024.105957.

Ahmadivala, M., Berthellemy, J., Orcesi, A., Mattrand, C., Gayton, N. and Yalamas, T. (2022), "A strategy for rib-to-deck crack propagation analysis and strengthening of orthotropic deck bridges", *Eng. Fail. Anal.*, **134**, 106057. https://doi.org/10.1016/j.engfailanal.2022.106057.

Alemdar, F., Nagati, D., Matamoros, A., Bennett, C. and Rolfe, S. (2014), "Repairing distortion-induced fatigue cracks in steel bridge girders using angles-with-plate retrofit technique. I: Physical Simulations", *J. Struct. Eng.*, **140**(5), 04014003. https://doi.org/10.1061/(ASCE)ST.1943-541X.0000876.

Al-Mosawe, A., Agha, M., Oraim, H. and Al-Mahadi, R. (2024), "Enhancing fatigue life of steel plates with CFRP laminate: Effects of curing temperature, stress range, and adhesive thickness", *J. Construct. Steel Res.*, **213**, 108352. https://doi.org/10.1016/j.jcsr.2023.108352.

Deng, Y., Liu, T.L., Cao, B.Y. and Li, A.Q. (2023), "Fatigue Strengthening for Rib-to-Deck Joint by Bonding Reinforcing Plates on the Deck Surface", *J. Bridge Eng.*, **28**(7), 04023040. https://doi.org/10.1061/JBENF2.BEENG-5617.

Fang, L., Fu, Z.Q., Ji, B.H. and Li, X.C. (2023), "The stiffness-degradation law of base metal after fatigue cracking in steel bridge deck", *Steel Compos. Struct.*, **47**(2), 239-251. https://doi.org/10.12989/scs.2023.47.2.239.

Fisher, J.M. and Barsom, J.M. (2016), "Evaluation of cracking in the rib-to-deck welds of the Bronx-Whitestone Bridge", *J. Bridge Eng.*, **21**(3), 04015065. https://doi.org/10.1061/(ASCE)BE.1943-5592.0000823.

Fu, Z.Q., Wang, Q.D., Ji, B.H. and Yuan-zhou Z.Y. (2017), "Rewelding repair effects on fatigue cracks in steel bridge deck welds", *J. Perform. Constr. Facil.*, **31**(6), 04017094. https://doi.org/10.1061/(ASCE)CF.1943-5509.0001083.

Fu, Z.Q., Ji, B.H., Wang, Y.X. and Xu, J. (2018), "Fatigue performance of rib-roof weld in steel bridge decks with corner braces", *Steel Compos. Struct.*, **26**(1), 103-113. https://doi.org/10.12989/scs.2018.26.1.103.

Guo, T., Liu, J., Deng, Y. and Zhang, Z.L. (2019), "Fatigue Performance of Orthotropic Steel Decks with FRP Angles: Field Measurement and Numerical Analysis", *J. Perform. Construct. Facil.*, **33**(4): 04019042. https://doi.org/10.1061/(ASCE)CF.1943-5509.0001308.

Hattori, M., Tateishi, K., Han-ji, T. and Shimizu, M. (2022), "Effect of UHPFRC overlay on fatigue cracks propagating from U-rib welds of orthotropic steel decks", *Int. J. Steel Struct.*, **22**(6), 1808-1816. https://doi.org/10.1007/s13296-022-00660-9.

Jiang, X., Lv, Z.L., Qiang, X.H. and Xu, Z.M. (2024), "Fatigue performance of root-to-throat cracks repaired by bonding steel: experimental and numerical investigations", *J. Constr. Steel Res.*, **212**, 108296. https://doi.org/10.1016/j.jcsr.2023.108296.

JTG D64 (2015), *Specifications for Design of Highway Steel Bridge*, CCCC Highway Consultants CO., LTD, Beijing, China.

Ke, L., Li, C.X., He, J., Lu, Y.J., Jiao, Y. and Liu, Y.M. (2021), "Fatigue evaluation and CFRP strengthening of diaphragm cutouts in orthotropic steel decks", *Steel Compos. Struct.*, **39**(4), 453-469. https://doi.org/10.12989/scs.2021.39.4.453.

Liu, J., Guo, T., Feng, D.M. and Liu, Z.X. (2018), "Fatigue performance of rib-to-deck joints strengthened with FRP

angles", *J. Bridge Eng.*, **23**(9), 04018060. https://doi.org/10.1061/(ASCE)BE.1943-5592.0001286.
Li, D.Z. (2018), "research on fatigue property and fatigue crack repairmethods of orthotropic steel bridge deck", M.S. Dissertation, Dalian University of Technology, Liaoning, China.
Merzoug, M., Boulenouar, A. and Benguediab, M. (2017), "Numerical analysis of the behaviour of repaired surface cracks with bonded composite patch", *Steel Compos. Struct.*, **25**(2), 209-216. https://doi.org/10.12989/scs.2017.25.2.209.
Oda, K., Ashikari, S. and Noda, NA. (2024), "Analysis method useful for calculating various interface stress intensity factors efficiently by using a proportional stress field of a single reference solution modeling", *Arch. Appl. Mech.*, **94**(4), 779-800. https://doi.org/10.1007/s00419-024-02540-6.
Okura, I. and Ishikawa, T. (2002), "Stop-hole conditions to prevent re-initiation of fatigue cracks", *Steel Compos. Struct.*, **2**(6), 475-488. https://doi.org/10.12989/scs.2002.2.6.475.
Qiang, X.H., Chen, L.L., Jiang, X. and Dong, H. (2023), "Experimental study on anchorage and activation performance of Fe-SMA strips for structural reinforcements", *Constr. Build. Mater.*, **401**, 132961. https://doi.org/10.1016/j.conbuildmat.2023.132961.
Russian, O., Belarbi, A. and Dawood, M. (2022), "Effect of surface preparation technique on fatigue performance of steel structures repaired with self-stressing SMA/CFRP patch", *Compos. Struct.*, **280**, 114968. https://doi.org/10.1016/j.compstruct.2021.114968.
Wang, B.H., Lu, P.M. and Shao, Y.H. (2015), "Research on rib-to-diaphragm welded connection by means of hot spot stress approach", *Steel Compos. Struct.*, **18**(1), 135-148. https://doi.org/10.12989/scs.2015.18.1.135.
Wang, Q.D., Ji, B.H., Gao, T. and Fu, Z.Q. (2021), "Effective-notch-stress-based fatigue evaluation of rib-deck welds integrating the full-range S-N curve concept", *J. Constr. Steel Res.*, **179**, 106541. https://doi.org/10.1016/j.jcsr.2021.106541.
Wang, H.T., Wu, G., Pan, Y.Y. and Zakari, HM. (2019), "Stress intensity factors for double-edged cracked steel beams strengthened with CFRP plates", *Steel Compos. Struct.*, **33**(5), 629-640. https://doi.org/10.12989/scs.2019.33.5.629.
Ya, S., Yamada, K. and Ishikawa, T. (2011), "Fatigue evaluation of rib-to-deck welded joints of orthotropic steel bridge deck", *J. Bridge Eng.*, **16**(4), 492-499. https://doi.org/10.1061/(ASCE)BE.1943-5592.0000181.
Yang, H.B., Qian, H.L. and Wang, P. (2021), "Fatigue property analysis of U rib-to-crossbeam connections under heavy traffic vehicle load considering in-plane shear stress", *Steel Compos. Struct.*, **38**(3), 271-280. https://doi.org/10.12989/scs.2021.38.3.271.
Zhou, J.G. and Xu, Z.M. (2021), "Research on non-damage repair technology for fatigue crack of steel box girder bridge", *Proceedings of the 10th International Conference on Bridge Maintenance*, Sapporo, Japan, April. https://doi.org/10.1201/9780429279119-230.
Zhu, A.Z., Ouyang, S.J., Chen, Y.K. and Sun, Y. (2022), "Fatigue test and life evaluation of rib-to-deck connections in orthotropic steel bridge decks", *J. Construct. Steel Res.*, **197**, 107442. https://doi.org/10.1016/j.jcsr.2022.107442.
Zhu, Z.W., Xiang, Z. and Li, J.P. (2020), "Fatigue damage investigation on diaphragm cutout detail on orthotropic bridge deck based on field measurement and FEM", *Thin-Wall. Struct.*, **157**, 107106. https://doi.org/10.1016/j.tws.2020.107106.